Provided for non-commercial research and education use.
Not for reproduction, distribution or commercial use.

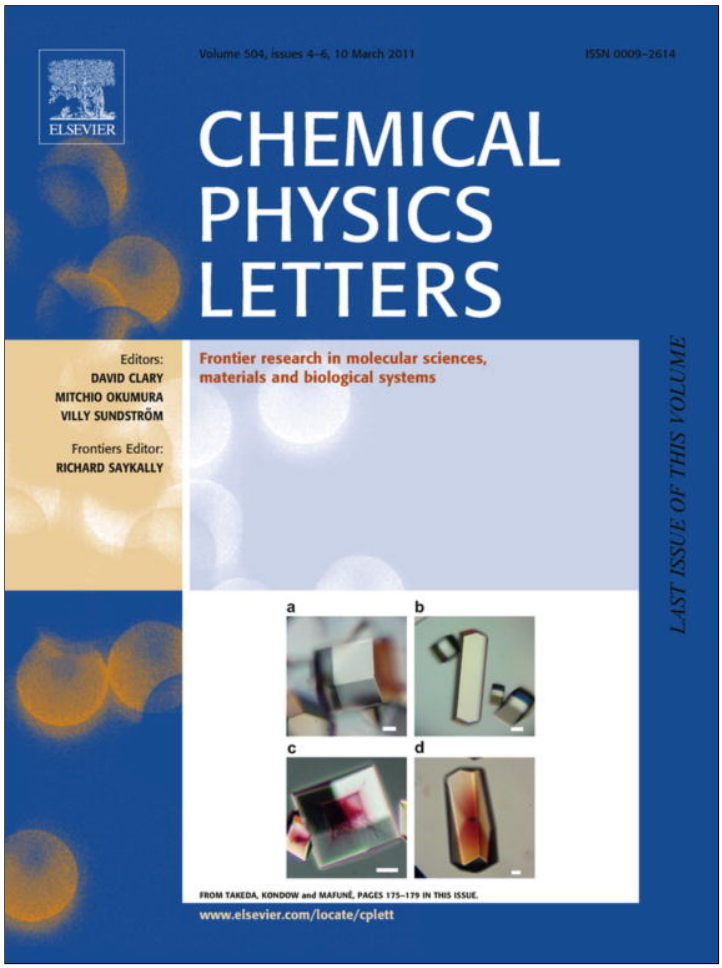

This article appeared in a journal published by Elsevier. The attached copy is furnished to the author for internal non-commercial research and education use, including for instruction at the authors institution and sharing with colleagues.

Other uses, including reproduction and distribution, or selling or licensing copies, or posting to personal, institutional or third party websites are prohibited.

In most cases authors are permitted to post their version of the article (e.g. in Word or Tex form) to their personal website or institutional repository. Authors requiring further information regarding Elsevier's archiving and manuscript policies are encouraged to visit:

http://www.elsevier.com/copyright

Author's personal copy

Chemical Physics Letters 504 (2011) 153–158

Contents lists available at ScienceDirect

Chemical Physics Letters

journal homepage: www.elsevier.com/locate/cplett

Density functional theory for differential capacitance of planar electric double layers in ionic liquids

De-en Jiang [a,*], Dong Meng [b], Jianzhong Wu [b,*]

[a] Chemical Sciences Division, Oak Ridge National Laboratory, Oak Ridge, TN 37831, USA
[b] Department of Chemical and Environmental Engineering, University of California, Riverside, CA 92521, USA

ARTICLE INFO

Article history:
Received 8 November 2010
In final form 27 January 2011
Available online 1 February 2011

ABSTRACT

The differential capacitance of electric double layers in ionic liquids and its correlation with the surface charge density, ion size and concentration are studied within the framework of the classical density functional theory (DFT). As prescribed by previous analytical theories, DFT is able to reproduce the transition in the differential capacitance versus the surface potential curve from the 'camel' shape to the 'bell' shape when the ionic density increases. However, DFT predicts alternating layers of cations and anions at the charged surface that cannot be described by the classical Gouy–Chapman–Stern model and its modifications.

© 2011 Elsevier B.V. All rights reserved.

1. Introduction

The electric double layer (EDL) lies at the heart of our understanding of the interfacial behavior of ionic liquids (IL) at a charged surface. This interface is especially important for energy storage in the so-called electric-double-layer capacitors or more conveniently, supercapacitors. Recent experimental breakthroughs in achieving high-capacitance and fast-charging supercapacitors highlight the importance of controlling pore sizes, particle morphology, and materials assembly [1–3]. The emergence of IL as a new type of energy carrier also brought new life to theoretical investigations of electrolyte/electrode interface in non-aqueous environments [4].

The theory of the EDL in ionic liquids advanced greatly after two complementary analytical studies [5,6] that yield similar equations for the differential capacitance of the electrolyte/electrode interface. The work by Kornyshev was focused on ionic liquid/metal interfaces [5], and that by Kilic et al. targeted general electrolyte/metal interfaces [6]. Both studies predicted that an increase of the ionic concentration would result in a transition from the 'camel' (or M shape) to the 'bell' shape when the differential capacitance is plotted as a function of the surface potential or the applied electric potential. By contrast, the Gouy–Chapman theory predicts only a U-shaped differential capacitance curve at all ionic concentrations. Follow-on experimental work was conducted and was able to produce both the camel and bell shapes in the differential capacitance curve for IL/electrode interfaces [7–11]. However, experimental results are highly sensitive to the substrate details, electrolyte condition, and temperature [12].

A number of theoretical studies and simulations have ensued after the analytical works by Kornyshev [5] and by Kilic et al. [6]. For example, Oldham applied the Gouy–Chapman–Stern (GCS) model to IL/metal interfaces and showed that the GCS model also gave rise to the bell-shaped differential capacitance curve [13]. Lamperski et al. examined the transition from the camel shape to the bell shape with an exclusion-volume-corrected Poisson–Boltzmann equation as well as the modified Poisson–Boltzmann theory which treats both fluctuation and exclusion volume terms [14]. Fedorov and Kornyshev used both Monte Carlo (MC) and molecular dynamics (MD) simulations to confirm Kornyshev's previous theoretical predictions and examined the effects of ion-size disparity on the interfacial behavior [15,16]. Whereas the classical GCS model is now well documented to be inadequate to describe characteristics of electrode/ionic liquid interfaces, there is still controversy regarding the origin of the camel shape for the IL/metal interface. MC simulations by Fedorov et al. and by Georgi et al. showed that the camel shape evolves as a result of neutral tails in the cation of the IL [17,18]. However, MD simulations by Trulsson et al. showed that the camel shape in the differential capacitance is attributed to the loss of van der Waals attractions among the ionic species near the electrode [19]. Lauw et al. examined the EDL at the IL/electrode interface with a numerical self-consistent mean-field theory and showed that including an effective dielectric constant may also lead to the camel shape [20]. Vatamanu et al. performed atomistic MD simulations of a room-temperature ionic liquid at graphite electrodes and investigated the dependences of the differential capacitance on the electric potential and temperature; they also obtained the camel-shaped curve [21].

It was shown in very recent MC simulations [22] that the bell-shaped curve appears for a good metal electrode due to the strong attraction between ions and their image charges, while the camel-

* Corresponding authors.
E-mail addresses: jiangd@ornl.gov (D.-e. Jiang), jwu@engr.ucr.edu (J. Wu).

0009-2614/$ - see front matter © 2011 Elsevier B.V. All rights reserved.
doi:10.1016/j.cplett.2011.01.072

Author's personal copy

shaped curve appears for the semi-metal electrode (such as glassy carbon) because the finite screening length shifts the reflection plane for the image charges into the electrode and reduces the attraction. Moreover, Outhwaite et al. showed by using a modified Poisson–Boltzmann theory that the effect of the image charges is substantial at low temperatures [23]. However, experimentally, the camel shape also appeared on a good metal [10]. Besides, the experimental results on carbon electrodes are controversial: Locket et al. reported the camel shape on glassy carbon [7], while Ohsaka et al. observed only the U-shape on glassy carbon and graphite [9–11]. It appears that the shape of the differential capacitance depends on many other factors including the image charge effects.

In recent years classical density functional theory (DFT) has evolved into a powerful and efficient computational tool to study the structure and phase behavior of complex molecular systems [24,25]. Although DFT has been used before to examine the structures of electric double layers in aqueous systems [26–28], we are unaware of any published work on application of DFT to ionic liquids. A main purpose of this Letter is to use DFT to investigate the differential capacitance curve and its correlation with the point of zero charge (PZC) and various ion–ion and ion–electrode interactions. At the fundamental level, we ask: (1) Can we reproduce the transition from the camel to bell shape in the differential capacitance curve? (2) What are the microscopic structures of the IL interfaces, especially in the high ionic concentration regime? (3) How does the size disparity in cations and anions affect the differential capacitance curve? Answering these questions would pave the way for further applying DFT to studying differential capacitance of EDLs at more complicated and realistic substrate geometries and to systems at larger length scales.

2. Method

We use a primitive model of electrolyte solutions to represent ionic liquids in a 'good' co-solvent, i.e., the dielectric behavior of the solvent is the same as that of the pure ionic liquid such that the cations and anions are fully dissociated and the thermodynamic nonideality is dominated by electrostatic interactions. In addition, we assume that the EDL is represented by the distributions of cations and anions near a charged planar surface with the dielectric constant identical to that of the solvent. The cations and anions are modeled as charged hard spheres and the solvent as a continuum of dielectric constant ϵ. Within these highly idealistic assumptions, the pair interaction potential between ions is given by

$$u_{ij}(r) = \begin{cases} \infty & r < (\sigma_i + \sigma_j)/2 \\ Z_i Z_j e^2/\varepsilon r & r \geqslant (\sigma_i + \sigma_j)/2 \end{cases} \tag{1}$$

where r is the center-to-center distance, σ_i and Z_i are the diameter and valence of ion i, respectively, and e represents the unit charge. The electrode is modeled as a rigid wall; the external potential of the charged wall acting on the ions is given by

$$V_i^{ext}(z) = \begin{cases} \infty & z < \sigma_i/2 \\ -2\pi Z_i e Q z/\varepsilon & z \geqslant \sigma_i/2 \end{cases} \tag{2}$$

where Q stands for the surface charge density, and z is the perpendicular distance from the surface. While the surface is often considered as a metal electrode in a number of previous investigations, we assume that it consists of a high-surface-area material (such as porous carbon used in supercapacitors [1]) with a dielectric constant comparable to that of the ionic liquid. In that case, we may ignore the image charges due to the discontinuity of the dielectric constant at the boundary.

Given the bulk ionic concentration and the surface charge density, the density profiles of cations and anions in the EDL, $\rho_\alpha(r), \alpha = \pm$, are solved by minimization of the grand potential

$$\Omega = \sum_{\alpha=+,-} \int d\mathbf{r} \rho_\alpha(\mathbf{r}) \{k_B T[\ln \rho_\alpha(\mathbf{r}) - 1] + V_\alpha^{ext}(\mathbf{r}) - \mu_\alpha\} + F^{ex}[\rho_+(\mathbf{r}), \rho_-(\mathbf{r})] \tag{3}$$

where k_B denotes the Boltzmann constant, T is the absolute temperature, μ_α is the chemical potential of ion α, and F^{ex} is the excess intrinsic Helmholtz energy functional arising from the electrostatic interactions and excluded volume effects of ions. See Ref. [28,29] for the exact expression of F^{ex} and for the numerical details to solve $\rho_\alpha(r), \alpha = \pm$.

From the density profiles, we can calculate the mean electrostatic potential (MEP) in the EDL by integrating the Poisson equation

$$\psi(z) = \frac{4\pi}{\varepsilon} \int_z^\infty dz'(z - z') \sum_i z_i e \rho_i(z') \tag{4}$$

Eq. 4 allows us to determine the surface electrostatic potential and the point of zero charge (PZC), i.e., a position where the electrical charge density is zero. By plotting the surface charge density against the surface potential, we obtain the differential capacitance numerically.

3. Results and discussion

We first consider a simple case where cations and anions have the equal diameter (0.6 nm) and the solvent dielectric constant is 12.5, typical for an ionic liquid [30]. Figure 1 shows the DFT predictions on how the surface charge density changes with the surface potential for different reduced densities of the room-temperature ionic liquid ($\rho_+\sigma^3$). Because cations and anions have the same size, the plot would be symmetric regarding the origin if one would extend the calculation to the negative surface potential. While the surface charge density increases monotonically with the surface potential, we observe noticeable change of the curvature as the io-

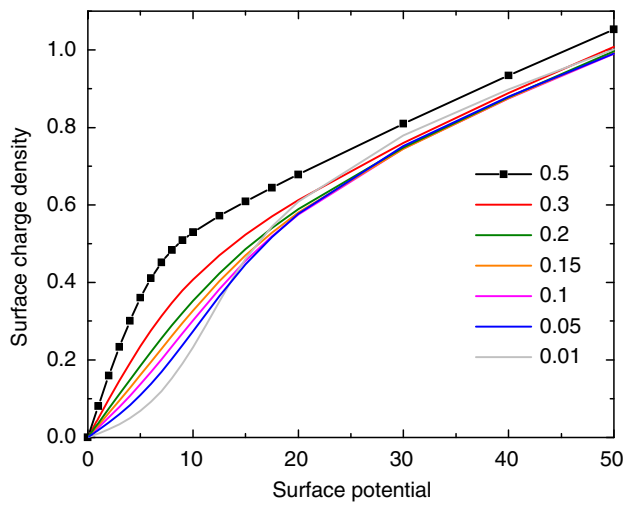

Figure 1. The charge density ($Q\sigma^2/e$) of a planar surface as a function of the surface potential ($\psi e/k_B T$) at various reduced bulk densities ($\rho_+\sigma^3$) of a model ionic liquid. Here both the cations and anions are monovalent and have the same hard-sphere diameter (σ = 0.6 nm); the solvent dielectric constant is 12.5 and temperature is at 298 K. DFT data points are shown for only $\rho_+\sigma^3$ = 0.5; only a line is used for the other densities. Reduced bulk density can be converted to mol/L by multiplying a factor of 7.7. The surface potential can be converted to volts by multiplying a factor of 1/39.

Author's personal copy

nic density increases. At all ionic densities, the surface charge density increases linearly at high surface potentials and the slope is nearly independent of the ionic concentration. As discussed later, this linear behavior can be explained in terms of lattice saturation [5].

The differential capacitance of the EDL is obtained by a derivative of the surface charge density with respect to the surface potential. Figure 2 shows both the positive and the negative branches of the differential capacitance at the same conditions as those in Figure 1. We see that at low ionic densities, the differential capacitance shows a minimum at zero surface potential and a maximum (or a peak) at a non-zero surface potential. Over the entire range (from negative to positive potential) the differential capacitance curve exhibits two symmetric peaks, which affirms the so-called camel shape of the differential capacitance [5]. At high ionic densities, the differential capacitance reaches a maximum at zero surface potential, giving the so-called bell-shaped curve [5]. From the camel shape to the bell shape, we may identify a smooth cross-over density at $\rho_+\sigma^3 = 0.2$. At this density, the differential capacity curve shows an inflection point at the zero potential. Apparently, our DFT calculations were able to reproduce the transition from the camel shape to the bell shape predicted by earlier analytical theories [5,6].

The camel-shaped curve of the differential capacitance can be understood from the GCS model. The local-minimum region between the two peaks is dominated by the diffuse layer whose differential capacitance follows the Gouy–Chapman model and hence gives a U shape. With increasing electric potential, a compact Stern layer is formed at the electrode surface, as shown in Figure 3 (at $\psi^*=\psi e/k_BT = 10$). Without specific adsorption, the total differential capacitance (C_t) is related to the differential capacities of the compact layer (C_c) for the ion-wall exclusion region and the diffuse layer (C_d):

$$\frac{1}{C_t} = \frac{1}{C_c} + \frac{1}{C_d}. \tag{5}$$

Because C_d increases with the electric potential while C_c is relatively constant, C_d becomes much greater than C_c at sufficiently high electric potential. In that case, C_t will be dominated by C_c. After the

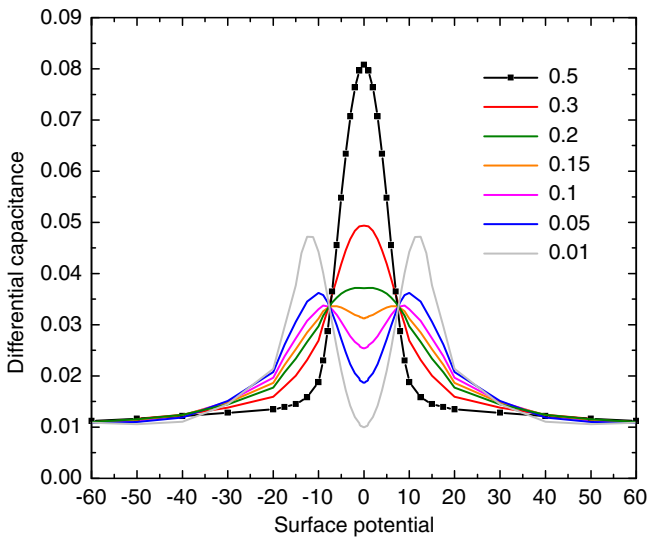

Figure 2. Differential capacitance versus surface potential ($\psi^* = \psi e/k_BT$) at various reduced bulk densities ($\rho_+\sigma^3$) of a model ionic liquid for systems the same as those in Figure 1. Reduced bulk density can be converted to mol/L by multiplying a factor of 7.7. The dimensionless differential capacitance can be converted to μF/cm^2 by multiplying a factor of 1733; the surface potential can be converted to volts by multiplying a factor of 1/39.

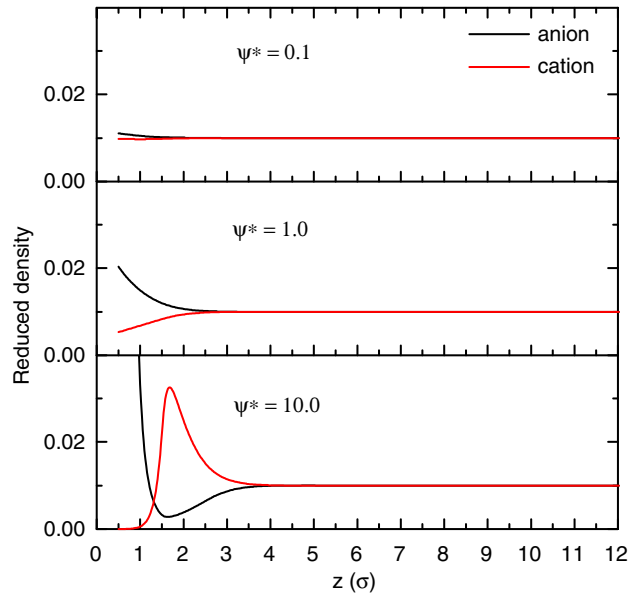

Figure 3. Density profiles of cations (red line) and anions (black line) within the electric double layer of the model ionic liquid at bulk density $\rho_+\sigma^3 = 0.01$ under three different surface potentials ($\psi^* = \psi e/k_BT$). The parameters for the ionic liquid are the same as those in Figure 1. Here z is the distance from the charged wall into the ionic liquid ($\sigma = 0.6$ nm); surface potential (ψ^*) can be converted to volts by multiplying a factor of 1/39.

maximum is reached, the decaying of C_d is dictated by lattice saturation as discussed by Kornyshev and coworkers [5,16]. As a result of the maximum in the local ionic concentration (c_{max}, including both cations and anions) and charge neutrality (the charge on the electrode is balanced by the integrated charge on the double layers), C_d decays with the square root of the potential [5,16]. More specifically, the capacitance of the EDL at high surface potentials can be approximated by

$$C_d \approx \sqrt{\frac{\varepsilon e^2 c_{max}}{8\pi k_B T}} \frac{1}{\sqrt{|\psi|}} \tag{6}$$

According to the the Gouy–Chapman–Stern model, C_c is independent of $|\psi|$. As a result, Eqs. 5 and 6 predict that C_t^{-1} should be linearly dependent on $|\psi|^{1/2}$. Such linear relation is affirmed by the DFT calculation as shown in Figure 4 where we plotted C_t^{-1} against $|\psi^*|^{1/2}$ for two densities at large $|\psi^*|$ (>40). Therefore, we conclude that the decaying wing in the camel shape can be explained by lattice saturation [5,16]. The camel shape arises from initial compression of the liquid at small voltages, which provides the rising branches of the capacitance, and then termination at larger voltages due to the onset of lattice saturation [5].

Figures 3 and 5 show the density profiles of cations and anions at different surface electrostatic potentials. At low IL concentration and small surface potential, cations and anions are distributed almost uniformly throughout the system. As expected, anions are accumulated at and cations are depleted from the surface as the electrostatic potential increases. At high surface potential, however, accumulation of anions is also seen near the surface, contradictory to the predictions of the GCS model. The density profiles are noticeably different at high IL concentrations (Figure 5). In this case, the ionic excluded volume effects lead to strong oscillatory distributions of both cations and anions. At close to zero surface electrostatic potential ($\psi^* = 0.1$), multiple layers of cations and anions are already formed near the surface, and each layer contains approximately equal densities of cations and anions. This layered structure was also observed in atomistic MD simulations [31]. Be-

Author's personal copy

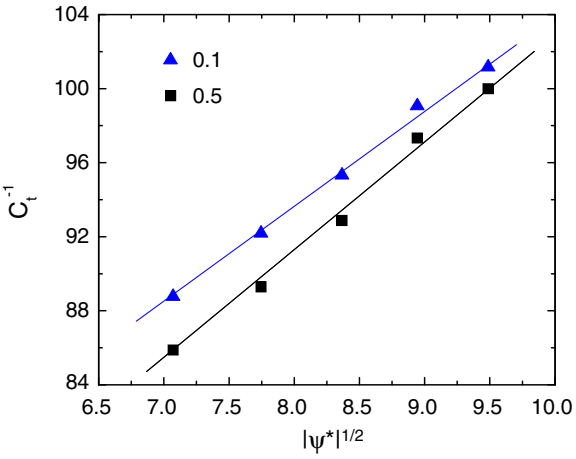

Figure 4. Inverse differential capacitance (C_t^{-1}) versus the square root of the reduced surface potential ($|\psi^*|^{1/2} = |\psi e/k_BT|^{1/2}$) for systems the same as those in Figure 1 at two reduced bulk densities (0.1 and 0.5), which be converted to mol/L by multiplying a factor of 7.7. The dimensionless C_t^{-1} can be converted to $(\mu F/cm^2)^{-1}$ by multiplying a factor of 1/1733; $|\psi^*|^{1/2}$ can be converted to $(volts)^{1/2}$ by multiplying a factor of 0.16.

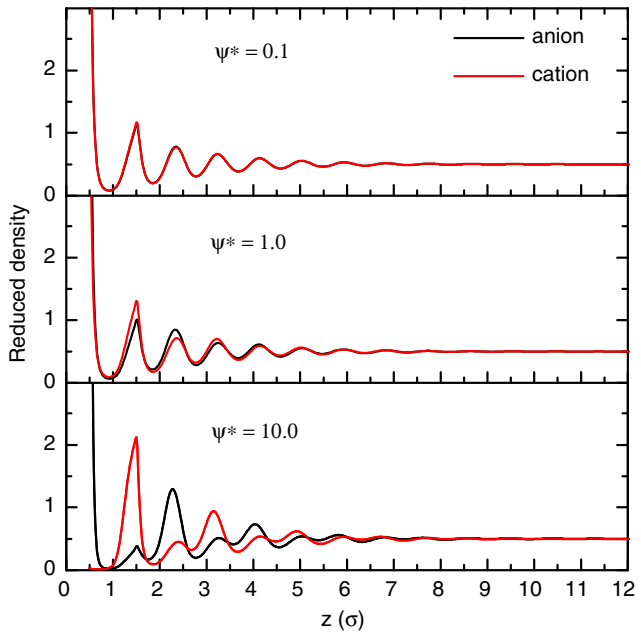

Figure 5. Density profiles of cations (red line) and anions (black line) within the electric double layer of the model ionic liquid at bulk density $\rho_+\sigma^3 = 0.5$ under three different surface potentials ($\psi^* = \psi e/k_BT$). The parameters for the ionic liquid are the same as those in Figure 1. Here z is the distance from the charged wall into the ionic liquid ($\sigma = 0.6$ nm; surface potential (ψ^*) can be converted to volts by multiplying a factor of 1/39. (For interpretation of the references to color in this figure legend, the reader is referred to the web version of this article.)

cause the Poisson–Boltzmann equation ignores the ion size, it cannot capture the oscillatory densities due to the excluded volume effect. This explains why the GCS model [Eq. 5] is not able to reproduce the bell-shaped differential capacitance curve. With increasing potential such as to $\psi^* = 1.0$, the positive charges on the surface is over-compensated by the net negative charges on the first layer, so the second layer gives a net positive charge. The layer-by-layer structure extends several layers into the bulk region (namely, farther away from the surface) [5]. Figure 5 also shows that, at high surface potential ($\psi^* = 10$), co-ions (cations) are repelled from the first layer while the counter-ions (anions) are pushed out of the second layer, and so on. As a result, alternating layers of cations and anions are formed near the electrode surface.

The density profiles shown in Figure 5 help explain the bell shape of the differential capacitance at high ionic densities. In the absence of chemisorption, the maximum capacitance coincides with PZC, but, as discussed and shown in Ref. [5,15], this is true only when cations and anions have identical size. As shown in Figure 6, the location of the capacitance maximum would shift toward positive potentials as the size ratio of cations and anion increases [5,13,14]. At high ion densities, both cations and anions are densely packed near the electrode surface, preventing counterions getting close to the electrode. With increasing surface potential, the net numbers of counterions have to extend to several layers into the bulk, effectively increasing the thickness of the EDL and hence decreasing the capacitance. At high surface potential, the decaying wing of the bell shape shares the same physics of lattice saturation as that of the camel shape [16]; namely, the differential capacitance decreases linearly with $|\psi|^{-1/2}$ (Figure 4).

Now we examine how the shape of the differential capacitance changes as we increase the ionic density at a fixed cation/anion size ratio ($\sigma_+ = 0.6$ nm, $\sigma_- = 0.3$ nm). At low ionic density ($\rho_+\sigma_+^3 = 0.1$), the symmetric double peaks in the differential capacitance curve for the equal-size case becomes asymmetric with one peak significantly higher than the other (Figure 7). The peak differential capacity is higher at a positively charged surface due to the smaller size of anions. Likewise, at high ionic density ($\rho_+\sigma_+^3 = 0.4$), the bell shape becomes asymmetric and the peak shifts to the positive surface potential. We also observe a slight shift of the PZC when the sizes of two ions differ. For example, for the bulk density of cations ($\rho_+\sigma_+^3 = 0.4$), PZC is at ~ -1 unit (indicated by the dashed line in Figure 7). At an intermediate density, the smaller peak in the camel-shaped differential capacitance curve is hard to discern and appears as a small hump (indicated by the arrow in Figure 7). Qualitatively, the effect of size disparity on the differential capacitance predicted from our DFT calculations agrees well with the MD simulations by Fedorov et al. [15]

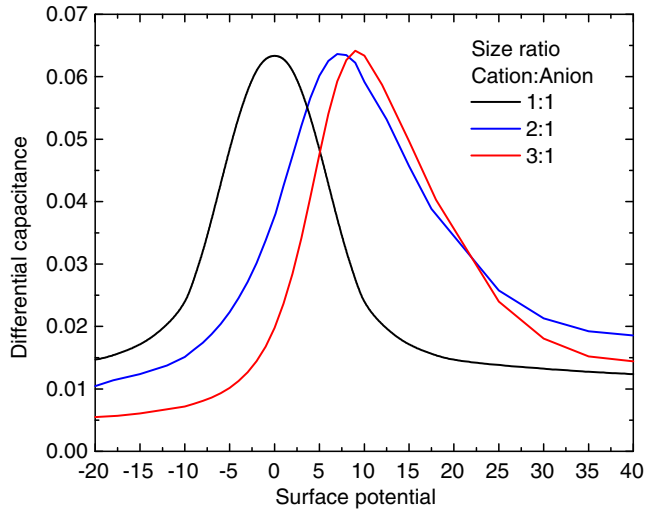

Figure 6. Differential capacitance versus surface electric potential for electric double layers of an asymmetric ionic liquid with increasing cation/anion size ratio (the reduced bulk density is constant for all three cases, $\rho_+\sigma_+^3 = 0.4$). The solvent dielectric constant is 12.5 and temperature is 298 K. Differential capacitance on the y-axis is in arbitrary units as the curves are scaled to make a better comparison for the shift in the position of the maximum. Dimensionless surface potential (ψ^*) can be converted to volts by multiplying a factor of 1/39.

Author's personal copy

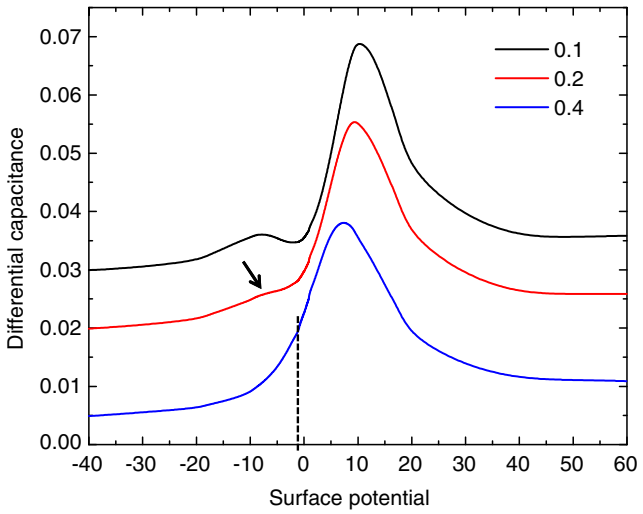

Figure 7. Differential capacitance versus surface potential for electric double layers of an asymmetric ionic liquid at various bulk densities ($\rho_+\sigma_+^3$). Here the diameter of cations is $\sigma_+ = 0.6$ nm, the diameter of anions is $\sigma_- = 0.3$ nm. The solvent dielectric constant is 12.5 and temperature is 298 K. Reduced bulk density can be converted to mol/L by multiplying a factor of 7.7. Differential capacitance on the *y*-axis is in arbitrary units as the curves are shifted vertically to make a better comparison. Dimensionless surface potential (ψ^*) can be converted to volts by multiplying a factor of 1/39.

4. Conclusions and discussion

In summary, we have investigated the differential capacitance of electric double layer in solutions of ionic liquids by using the classical density functional theory (DFT). The electrolytes are modeled as charged hard spheres in a continuum dielectric medium. DFT predicts the camel shape curve at low ionic density and the bell-shaped curve at high ionic density as observed in experiments and as predicted by previous simulation and analytical theories. A cross-over density was also identified. In addition, DFT predicts alternating layers of cations and anions at high polarization for the high ionic density, which is relevant to the structures of ionic liquids at a charged substrate. Asymmetric shape of the differential capacitance curve was observed for cations and anions of different sizes. This work demonstrates that DFT is a useful and efficient computational tool for further exploring the electrolyte/electrode interface for incorporating more sophisticated electrolyte models and substrate geometries.

Although the primitive model discussed in this work is not able to capture the microscopic details, its relevance to realistic ionic liquids at a charged surface is justified. There are several reasons for this. First, the ion sizes we examined at 0.6 and 0.3 nm approximate those of common ionic liquid cations and anions [32,33]; the dielectric constant for the solvent (12.5) is also similar to those of several common ionic liquids [30]. From this perspective, we can compare our results to Kornyshev's analytical predictions for the IL/metal interface. To measure the lattice compression, Kornyshev introduced parameter $\gamma = 2\rho_0/\rho_{max}$, where ρ_0 is the bulk concentration and ρ_{max} is the maximal possible local concentrations of ions including both cations and ions. Based on the Poisson–Boltzmann lattice-gas model with the ion volumes accounted for, Kornyshev predicted that the transition in the differential capacitance curve from the camel shape to the bell shape happens at $\gamma = 1/3$, which corresponds to a reduced bulk density of 0.167. Interestingly, our DFT calculations gave a similar transition density at 0.2 (Figure 2). Moreover, as pointed out by Kornyshev, γ should be close to 1 for a densely packed ionic liquid, which corresponds to a bulk density of 0.5. In this case, our DFT results gave a bell shape as predicted by Kornyshev [5].

Experimental measurement of the differential capacity of ionic liquids has been pursued by several groups [7–9,11]. Various shapes have been observed, depending on the chemical specifics of the ionic liquid, the substrate charge density, and the temperature. Interestingly, the camel-shaped curve has been observed for the IL/electrode interface [7], though theory predicts that the bell shape is more likely. Several simulations tried to account for the camel shape at the IL/electrode interface, but at this point the origin is still in controversy. Adding neutral components to the ions [17,18], including van der Waals attraction [19], and taking into account effective dielectric constant [20] all were shown to lead to the camel shape. Most recently, it has been shown that incorporating the image charges in the simulations for a more realistic description of the conductive electrode leads to the camel shape for the EDL of IL near a semi-metal electrode [22]. Given that the DFT results based on the simple models for the electrode and the IL could reproduce well the transition of the camel shape to the bell shape, we expect that the DFT would allow us to efficiently dissect the roles of various factors leading to the camel shape as we use more sophisticated models, by adding van der Waals interactions, accounting for the effective dielectric constant, and taking into account the image charges for metal electrodes.

Besides the shape of the differential capacitance curve, it is also interesting to examine the structure of cations and anions at the IL/electrode interface. As pointed out earlier, the results from the DFT calculations for the bulk density at ionic density $\rho\sigma^3 = 0.5$ can be considered as a simulation of an ionic liquid of equal-ion size at 0.6 nm. At high ionic concentration and high surface electrostatic potential, DFT predicts alternating layers of cations and anions at the interface. This result agrees with recent observation of such layering inferred from X-ray reflectivity measurements of ionic liquids on a negatively charged sapphire surface [33,34] and from atomistic MD simulations [16,21,35,36].

Acknowledgements

This material is based upon work supported as part of the Fluid Interface Reactions, Structures, and Transport (FIRST) Center, an Energy Frontier Research Center funded by the U.S. Department of Energy, Office of Science, Office of Basic Energy Sciences under Award No. ERKCC61 (D.J.). Additional support (J.W.) is provided by the National Science Foundation (NSF-CBET-0852353). This research also used resources of the National Energy Research Scientific Computing Center, which is supported by the Office of Science of the U.S. Department of Energy under Contract No. DE-AC02-05CH11231.

References

[1] J. Chmiola, G. Yushin, Y. Gogotsi, C. Portet, P. Simon, P.L. Taberna, Science 313 (2006) 1760.
[2] P. Simon, Y. Gogotsi, Nat. Mater. 7 (2008) 845.
[3] J. Chmiola, C. Largeot, P.L. Taberna, P. Simon, Y. Gogotsi, Science 328 (2010) 480.
[4] M. Armand, F. Endres, D.R. MacFarlane, H. Ohno, B. Scrosati, Nat. Mater. 8 (2009) 621.
[5] A.A. Kornyshev, J. Phys. Chem. B 111 (2007) 5545.
[6] M.S. Kilic, M.Z. Bazant, A. Ajdari, Phys. Rev. E 75 (2007) 021502.
[7] V. Lockett, R. Sedev, J. Ralston, M. Horne, T. Rodopoulos, J. Phys. Chem. C 112 (2008) 7486.
[8] M.T. Alam, M.M. Islam, T. Okajima, T. Ohsaka, Electrochem. Commun. 9 (2007) 2370.
[9] M.T. Alam, M.M. Islam, T. Okajima, T. Ohsaka, J. Phys. Chem. C 112 (2008) 16600.
[10] M.M. Islam, M.T. Alam, T. Ohsaka, J. Phys. Chem. C 112 (2008) 16568.
[11] M.M. Islam, M.T. Alam, T. Okajima, T. Ohsaka, J. Phys. Chem. C 113 (2009) 3386.
[12] V. Lockett, M. Horne, R. Sedev, T. Rodopoulos, J. Ralston, Phys. Chem. Chem. Phys. 12 (2010) 12499.
[13] K.B. Oldham, J. Electroanal. Chem. 613 (2008) 131.
[14] S. Lamperski, C.W. Outhwaite, L.B. Bhuiyan, J. Phys. Chem. B 113 (2009) 8925.

Author's personal copy

[15] M.V. Fedorov, A.A. Kornyshev, J. Phys. Chem. B 112 (2008) 11868.
[16] M.V. Fedorov, A.A. Kornyshev, Electrochim. Acta 53 (2008) 6835.
[17] M.V. Fedorov, N. Georgi, A.A. Kornyshev, Electrochem. Commun. 12 (2010) 296.
[18] N. Georgi, A.A. Kornyshev, M.V. Fedorov, J. Electroanal. Chem. 649 (2010) 261.
[19] M. Trulsson, J. Algotsson, J. Forsman, C.E. Woodward, J. Phys. Chem. Lett. 1 (2010) 1191.
[20] Y. Lauw, M.D. Horne, T. Rodopoulos, F.A.M. Leermakers, Phys. Rev. Lett. 103 (2009).
[21] J. Vatamanu, O. Borodin, G.D. Smith, J. Am. Chem. Soc. 132 (2010) 14825.
[22] M.S. Loth, B. Skinner, B.I. Shklovskii, Phys. Rev. E 82 (2010) 056102.
[23] C.W. Outhwaite, S. Lamperski, L.B. Bhuiyan, Molecular Physics (2010) doi:10.1080/00268976.2010.519 731.
[24] J.Z. Wu, Aiche J. 52 (2006) 1169.
[25] J.Z. Wu, Z.D. Li, Annu. Rev. Phys. Chem. 58 (2007) 85.
[26] C.N. Patra, S.K. Ghosh, J. Chem. Phys. 117 (2002) 8938.
[27] Z.D. Li, J.Z. Wu, J. Phys. Chem. B 110 (2006) 7473.
[28] Y.X. Yu, J.Z. Wu, G.H. Gao, Chin. J. Chem. Eng. 12 (2004) 688.
[29] Y.X. Yu, J.Z. Wu, J. Chem. Phys. 117 (2002) 2368.
[30] Y.J. Min, M. Akbulut, J.R. Sangoro, F. Kremer, R.K. Prud'homme, J. Israelachvili, J. Phys. Chem. C 113 (2009) 16445.
[31] S. Wang, S. Li, Z. Cao, T.Y. Yan, J. Phys. Chem. C 114 (2010) 990.
[32] M. Ue, A. Murakami, S. Nakamura, J. Electrochem. Soc. 149 (2002) A1385.
[33] M. Mezger et al., J. Chem. Phys. 131 (2009) 094701.
[34] M. Mezger et al., Science 322 (2008) 424.
[35] M. Sha, G. Wu, Q. Dou, Z. Tang, H. Fang, Langmuir 26 (2010) 12667.
[36] G. Feng, J. Huang, B.G. Sumpter, V. Meunier, R. Qiao, Phys. Chem. Chem. Phys. 12 (2010) 5468.